ACS Energy LETTERS

http://pubs.acs.org/journal/aelccp

VIEWPOINT

Efficiency Limit of Perovskite/Si Tandem Solar Cells

Organometal-halide perovskite/Si tandem solar cells (TSCs) have been proposed as a promising candidate to surpass Si efficiency records. Since the first report of a perovskite solar cell in 2009,[1] their power conversion efficiency has rapidly increased to more than 20%.[2,3] In contrast, after 60 years of research, the power conversion efficiency of Si solar cells is slowly approaching the Auger-recombination-constrained Shockley−Queisser limit of 29.8%.[2,4] To further increase the power conversion efficiency while simultaneously reducing the cost per kWh, new strategies such as tandem configurations have to be applied. A TSC consists of two or more cells that are optically coupled by absorbing different parts of the incident spectrum. This allows for more efficient conversion of the broad-band solar spectrum. In a two-cell configuration, the high-energy region of the spectrum is absorbed by the top cell, whereas the transmitted low-energy light is absorbed by the bottom cell. Hybrid organic−inorganic perovskite-based cells are especially well-suited as a top cell for Si-based TSCs due to their high charge carrier mobility, high quantum yield, long diffusion length, sharp absorption edge, and large tunable band gap covering almost the entire solar spectrum.[5−8] Recently, it was shown that lead halide perovskites recycle light, meaning that power conversion efficiencies as high as those in GaAs-based solar cells might be feasible.[9]

Several analyses on the limiting efficiency of TSCs have been performed using detailed-balance calculations showing efficiencies up to 69.9% for an infinite number of subcells under 1 sun illumination.[10−16] A key factor for the power conversion efficiency of TSCs is the way that the subcells are connected. A perovskite/Si TSC can be assembled in a two-terminal series connection where current matching is required, in a configuration that is voltage-matched at the module level, or as an unconstrained three- or four-terminal configuration where both subcells are electrically independent (see Figure 1). Monolithically integrated two-terminal,[17−21] mechanically stacked four-terminal,[22−27] and spectrally split four-terminal[28,29] configurations have already been reported showing an increase of the overall efficiency compared to the Si cell alone. The highest reported efficiency is 28.0%,[29] exceeding the record Si single-junction efficiency of 25.6%.[30]

The three tandem configurations have an almost identical efficiency limit of about 45% under standard test conditions (AM1.5G, 1 kW/m^2, 25 °C). However, the TSC configurations place different constraints on the choice of band gap and the stability of the efficiency when the incident spectrum or cell temperature changes. The performance of the voltage-matched two-terminal and the four-terminal configurations are most stable against varying spectral conditions.[31,32] In contrast, the efficiency of the current-matched two-terminal configuration is the most stable against temperature changes.[33,34] These dependencies suggest a nontrivial relation of the overall power conversion efficiency with the environment.[35,36]

Here we analyze the theoretical efficiency limit of perovskite/Si TSCs, comparing all three assembly strategies with different perovskite band gaps under incident solar spectra measured in two different locations with distinctly different climate conditions. Spectral irradiance, ambient temperature, and relative humidity data were measured in Utrecht, The Netherlands (NL) and in Denver, Colorado, US (CO) in 2015 at an interval of 10 min during daylight hours. We use these spectra and the associated temperature to calculate the maximum efficiency of perovskite/Si TSCs via the detailed-balance limit for perovskite top cells of a 1.55 eV band gap and for the ideal perovskite band gap for the respective tandem configuration. Note that these calculations do not take any material specific parameters into account, which makes them valid for any material combination with the respective band gaps.

Limiting Efficiency for Various Tandem Configurations. In a thermodynamic consideration of detailed-balance, the maximum power conversion efficiency of Si single-junction solar cells with a perfect reflector on the back side of the cell is limited to 33.5% for the AM1.5G spectrum at 25 °C, considering only radiative recombination as a loss mechanism and unitary probability that photons with an energy above the band gap will produce one free charge carrier pair. This is commonly referred to as the Shockley−Queisser (SQ) limit.[37] The two main losses arise due to the broad nature of the solar spectrum; photons with an energy below the band gap are transmitted, and photons with an energy above the band gap generate hot carriers that thermalize to the band-edge.

The most common TSC configuration is the monolithically integrated two-terminal in which the top cell and the bottom cell are optically stacked and electrically connected in series. In this configuration, the voltage of both cells adds and the photocurrent is limited by the cell producing the lower current. Consequently, when changes in the solar spectrum generate a mismatch between the current generated in the two subcells, the overall efficiency is reduced. An alternative assembly for a TSC is the use of mechanically stacked cells in either a two- or four-terminal configuration. A mechanically stacked two-terminal module tandem consists of n series-connected Si bottom cells and m series-connected perovskite top cells. Thereby, the perovskite cells can be voltage-matched with the Si cells and electrically connected in parallel. In this configuration, the current of the perovskite cells and the Si cells add and the maximum conversion efficiency is limited by the cell producing the lower voltage. A parallel connection has

Received: September 2, 2016
Accepted: September 27, 2016
Published: October 3, 2016

DOI: 10.1021/acsenergylett.6b00405
ACS Energy Lett. 2016, 1, 863−868

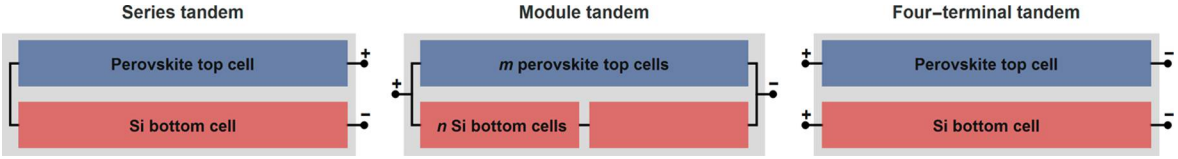

Figure 1. Schematic illustration of perovskite/Si TSC configurations. (Left) Monolithically integrated two-terminal tandem in which the perovskite top cell and the Si bottom cell are electrically connected in series. (Middle) Mechanically stacked two-terminal module tandem in which the perovskite top cells and the Si bottom cells are electrically connected in parallel. (Right) Four-terminal tandem in which the perovskite top cell and the Si bottom cell are electrically independent.

an advantage over a series connection because the open-circuit voltage (V_{OC}) changes only logarithmically with light intensity, whereas the short-circuit current (I_{SC}) changes linearly. A module tandem is therefore more stable against spectral variations.[31] Conversely, temperature changes affect mostly the voltage of a solar cell; hence, we expect the two-terminal module tandem to be the least stable against temperature changes (see the Supporting Information (SI) S1).

In an unconstrained four-terminal configuration, the top and bottom cells are electrically independent while still being optically coupled. A four-terminal tandem is not subject to either current or voltage matching, meaning that each subcell can maximize its power conversion efficiency independently. Consequently, a four-terminal TSC is expected to be the most stable against spectral and temperature changes.

To calculate the maximum efficiency for the different TSC configurations, SQ-type calculations with modifications similar to work of De Vos[10] and Strandberg[33] are used (see SI S2 for details). For efficiency calculations of the module tandem, the ideal ratio of the number of perovskite top cells to the number of Si bottom cells depends on the perovskite band gap. We set this ratio to 1/1.83 in order to match the efficiency-maximizing band gap of the perovskite cell in the module configuration to the efficiency-maximizing band gap of the perovskite cell in the four-terminal configuration. The limiting efficiencies for the two-terminal series tandem, the two-terminal module tandem, and the four-terminal tandem with a Si bottom cell (E_G = 1.12 eV) are shown in Figure 2. The limiting efficiency is 45.1% for

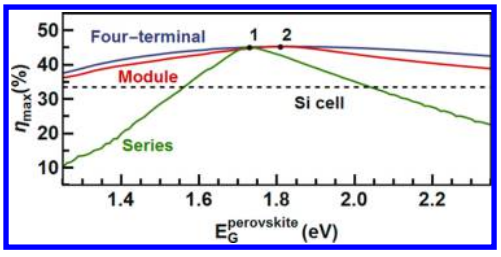

Figure 2. Efficiency limit of the three perovskite/Si TSC configurations with different band gaps of the top cell obtained by detailed-balance calculations under standard test conditions (AM1.5G, 1 kW/m^2, 25 °C). The optimal band gap for the top cell is 1.73 eV (point 1) for the series tandem and 1.81 eV (point 2) for the module and the four-terminal tandem. The dashed line corresponds to the SQ limit of Si.

the series tandem and 45.3% for the module and the four-terminal tandem under standard test conditions. Because the series tandem is subject to current matching, it features a narrow range of band gap combinations for the perovskite top cell from 1.57 to 2.04 eV where the efficiency limit exceeds the SQ limit of Si. The module tandem requires matching of the photovoltage, which poses a weaker constraint on the band gap compared to matching of the photocurrent,[31] while the electrically unconstrained four-terminal tandem allows for the broadest choice of band gap combinations. However, both the module and the four-terminal tandem configuration exceed the SQ limit of Si for perovskite top cells with a band gap above 1.12 eV.

Spectral Variations in the Netherlands and in Denver. Climate conditions determine the amount of solar radiation that reaches the earth and affect the performance of TSC devices based on the spectral and temperature response of the considered TSC configuration. According to the Köppen−Geiger climate classification,[38] NL has an oceanic climate with a narrow annual temperature range due to ocean currents, frequent precipitation, and variable weather, in many cases featuring an overcast sky. In contrast, CO has a steppe climate with lower precipitation and a broader annual temperature range, which on average is about 2 °C higher than that in NL.

The average photon energy (APE) is used to describe spectral irradiance distributions of measured spectra (see SI S3 for details). A high APE value corresponds to a blue-rich spectrum, whereas a low APE value corresponds to a red-rich spectrum. The APE was shown to be a suitable index to account for spectral irradiance variations.[39−42] The standard spectrum (AM1.5G) has an APE of 1.845 eV, calculated between 280 and 1107 nm, that is, for photons with an energy above the band gap of Si. The APE values of the annual average spectrum at both locations (1.840 eV in NL and 1.850 eV in CO) are fairly similar to the APE of the standard spectrum (see SI S4 for the annual average spectra). However, the irradiance of the annual average spectrum at both locations (249 W/m^2 in NL and 432 W/m^2 in CO) is much lower than the irradiance of the standard spectrum (1000 W/m^2).

Figure 3 illustrates the wide distribution in measured spectral variations in NL and in CO. Inset (1) in Figure 3a shows a measured spectrum during a sunny day at noon in summer, which closely follows the standard spectrum shaded in gray. Yet, only a small fraction of the measured spectra corresponds to the spectral distribution of the standard spectrum, indicating the importance of considering spectral variations governed by climate conditions for efficiency calculations of TSCs.

During winter months, spectra are considerably red-shifted compared to the standard spectrum. An exemplary spectrum measured during a winter morning is shown in Figure 3a, inset (2). This seasonal effect on the spectral irradiance is due to the higher air mass (AM) in winter than that in summer.[43] A higher AM indicates that the solar radiation covers a longer path through the Earth's atmosphere, which results in an increase in wavelength-dependent Rayleigh scattering and selective absorption of the solar radiation by atmospheric molecules.

The humidity also has a strong effect on the spectral distribution. Spectral irradiance data with a humidity higher than 90% are indicated in gray in Figure 3, with an exemplary

DOI: 10.1021/acsenergylett.6b00405
ACS Energy Lett. 2016, 1, 863−868

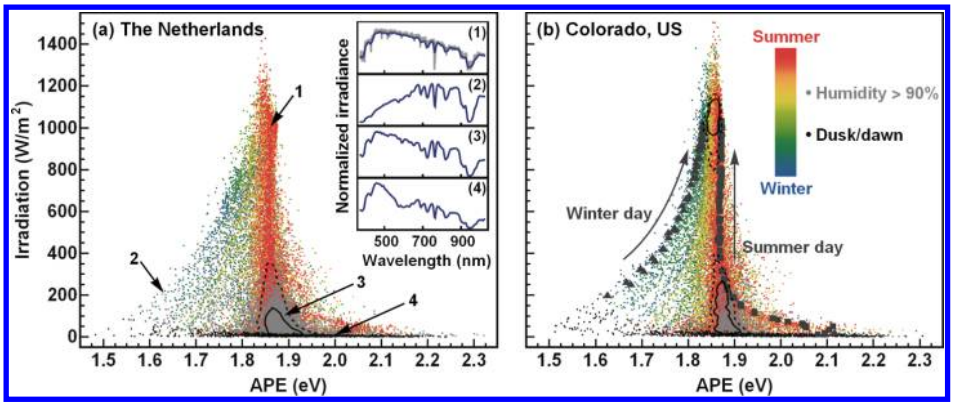

Figure 3. Spectral variations over the year 2015 in (a) NL[44] and in (b) CO[45]. The inset in (a) illustrates the wide variation in spectral distribution by means of exemplary solar spectra measured (1) at noon during the summer with the standard spectrum (AM1.5G) shaded in gray, (2) during a winter morning, (3) during a summer day with a high relative humidity, and (4) at dawn. The upright triangles and the squares in (b) correspond to the course of clear sky days measured in winter and in summer, respectively. The continuous and the dashed contour lines enclose 20 and 40% of the measured spectra, respectively.

spectrum measured during a summer day with a high relative humidity close to 100% shown in inset (3). A high relative humidity (often coincident with high cloud coverage and rain) results in a lower irradiation with an APE slightly blue-shifted with respect to the standard spectrum. This is due to increased absorption by water vapor molecules at 724, 824, 938, and 1120 nm[46] and due to reduced Rayleigh scattering as more of the solar radiation is Mie-scattered by water vapor droplets, which only weakly depends on the wavelength.[47]

Around dusk and dawn, spectra are blue-shifted with respect to the standard spectrum, as illustrated in Figure 3 by black dots for spectra measured up to 20 min before and after sunrise and sunset. The blue shift is due to absorption of solar radiation by the broad Chappuis band of ozone between 450 and 700 nm.[48] This appreciably affects the color of the spectra only when the sun is near the horizon, hence the path length of the solar radiation through the Earth's atmosphere is greatest.[49] An exemplary spectrum measured during dawn is shown in Figure 3a, inset (4).

Seasonal- and daytime-dependent variation of the spectrum is illustrated during the course of a clear sky winter (summer) day in Figure 3b by blue (red) triangles. In the winter, the spectrum is considerably red-shifted with respect to the standard spectrum. During the course of the day, the spectrum gradually blue shifts while the irradiation increases. When the day draws toward noon, the irradiation reaches its maximum and the APE is close to the standard spectrum. In the afternoon, the irradiation decreases and spectra undergo a red shift. Due to the lower AM in summer months, the spectrum does not show the red-shifted APE values and remains much closer to the standard spectrum while mainly the irradiation changes during the course of a clear sky summer day.

Site-Dependent Perovskite/Si Efficiency Limit. Calculated efficiency limits for perovskite/Si TSCs with the ideal band gap for the respective tandem configuration as a function of APE and irradiation are shown in Figure 4, taking spectral variations and temperature changes into account. Because the annually averaged APE of the two locations is similar to the one of the standard spectrum, the ideal band gap combinations for NL and CO are the same as those with the standard spectrum. Note that locations with an annually averaged APE dissimilar to the APE of the standard spectrum might have different ideal band gap combinations.

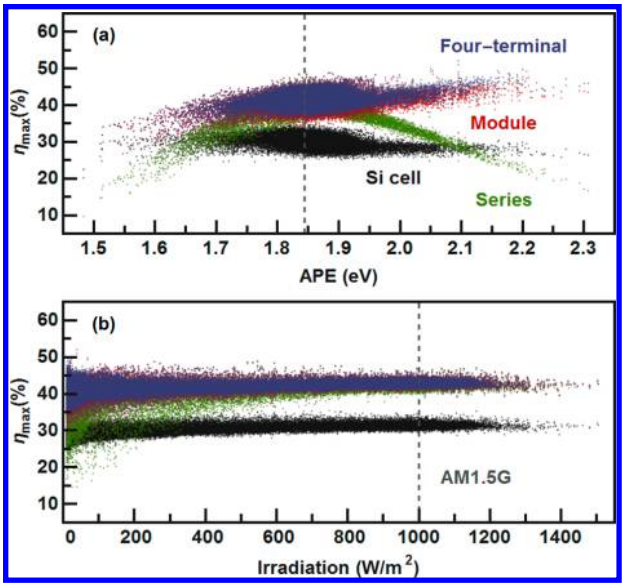

Figure 4. Efficiency limit of the three perovskite/Si tandem configurations and a single-junction Si cell under real illumination conditions as a function of (a) APE and (b) irradiation, obtained by detailed-balance calculations using data from both NL[44] and CO[45]. The dashed line indicates the APE and the irradiation of the standard solar spectrum (AM1.5G).

The limiting efficiency of a Si cell is influenced little by spectral changes. The limiting efficiency of TSCs on the other hand strongly depends on spectral and temperature changes. A shift in APE affects both the I_{SC} and the V_{OC} in the two subcells. Because the I_{SC} has a weaker dependence on the photon flux than the V_{OC}, the current-matched series tandem is most affected by spectral changes. At high APEs and low irradiations, the series tandem even features limiting efficiencies below the one of the single-junction Si cell. Furthermore, module and four-terminal TSCs show an increase in limiting efficiencies as the APE is increased because a larger part of the incident spectrum can be absorbed. The broad efficiency range for a given APE value is mostly due to different irradiation intensity because the efficiency logarithmically depends on the irradiation (see SI S5).

The intensity-weighted limiting power conversion efficiencies in NL and CO of spectral irradiance to electricity averaged over

DOI: 10.1021/acsenergylett.6b00405
ACS Energy Lett. 2016, 1, 863−868

the entire year are summarized in Table 1. The efficiency losses in realistic conditions compared to the standard test condition

Table 1. Power Conversion Efficiency Limit over an Entire Year for the Three Perovskite/Si Tandem Configurations and a Si Single-Junction Cell in NL[44] and CO[45] and under Standard Test Conditions (AM1.5G, 1 kW/m^2, 25 °C) Obtained by Detailed-Balance Calculations

	Si cell (%)	$E_G^{perovskite}$ (eV)	series (%)	module (%)	four-terminal (%)
standard test conditions	33.5	ideal	45.1	45.3	45.3
		1.55 eV	41.5	42.2	43.7
The Netherlands	31.1	ideal	41.5	42.4	42.5
		1.55 eV	38.3	39.6	40.9
Colorado, US	32.0	ideal	42.8	43.6	43.6
		1.55 eV	39.5	40.6	42.0

originating from spectral variations, temperature changes, and the use of a nonideal perovskite band gap are summarized in Figure 5. Due to a higher average irradiation in CO than in NL, efficiency losses are generally higher in NL. The series tandem performs somewhat worse compared to the module and the four-terminal tandem due to its sensitivity to spectral changes. This effect is more pronounced in NL than that in CO due to stronger changes in the spectral shape. Limiting efficiencies of TSCs furthermore decrease by up to 0.3% because of temperature changes. In total, the respective maximum annual energy yields for a perovskite/Si TSC in NL and in CO are 531 and 893 kWh/m^2 for a series tandem, 543 and 910 kWh/m^2 for a module tandem, and 544 and 911 kWh/m^2 for a four-terminal tandem, respectively.

Up to now, we assumed the ideal band gap for the perovskite subcells. The limiting efficiency of perovskite/Si TSCs with the commonly used methalyammonium lead iodide ($MAPbI_3$) with a band gap of 1.55 eV is somewhat lower. A series tandem with a nonideal perovskite band gap strongly depends on the optical thickness of the perovskite top cell because an optically thick absorber does not achieve current matching (see SI S6). We therefore set the absorption of the top cell to 80% in order to maximize the efficiency of the series tandem with $MAPbI_3$ as a top cell. In this configuration, we observe similar trends as those for the ideal band gap (Figure 5b), with an additional penalty for the nonideal band gap between 3.5 (four-terminal) and 8.1% (series tandem). The limiting efficiency of a perovskite/Si series tandem with optically thick $MAPbI_3$ is only 30.6% in NL and 31.3% in CO, taking only spectra changes into account. Consequently, perovskite/Si TSCs with optically thick $MAPbI_3$ should be built in either module or four-terminal configuration in order to surpass the SQ limit of Si.

We note that in a realistic situation individual subcells might be affected by stability issues or changing outdoor illumination conditions such as partial shading, which has a direct influence on the performance of TSCs. In particular, the series tandem strongly depends on the performance of individual subcells because the I_{SC} is limited by the subcell generating the lowest current. In addition, perovskite solar cells are currently farther from their efficiency limit than the heavily optimized silicon cells,[2] and calculations like the ones shown here should be performed whenever these tandem cells are to be employed on a large scale, for the particular location with realistic device parameters.

In summary, we have analyzed the influence of outdoor illumination conditions on the limiting efficiency of different perovskite/Si TSC configurations. The efficiency of perovskite/Si TSCs is strongly affected by spectral and temperature changes. Consequently, weather conditions at the specific site of deployment should be taken into account when designing perovskite/Si TSCs. Among all of the perovskite/Si TSC configurations, the current-matched series tandem is most affected by spectral variations and the use of a nonideal perovskite band gap. The impact of climate conditions on the limiting efficiency is primarily evident at low irradiations that comprise a significant amount of solar spectra measured throughout a year. These results indicate that perovskite/Si TSCs at different locations may require different tandem configuration and/or perovskite band gaps in order to minimize the cost per kWh. We show that by using a perovskite top cell with the ideal band gap for the respective tandem configuration, perovskite/Si TSCs with power conversion efficiency limits above 41% are possible for all three tandem configuration even at nonideal climate conditions.

Moritz H. Futscher
Bruno Ehrler*
Center for Nanophotonics, FOM Institute AMOLF, Science Park 104, 1098 XG Amsterdam, The Netherlands

■ ASSOCIATED CONTENT

Supporting Information

The Supporting Information is available free of charge on the ACS Publications website at DOI: 10.1021/acsenergylett.6b00405.

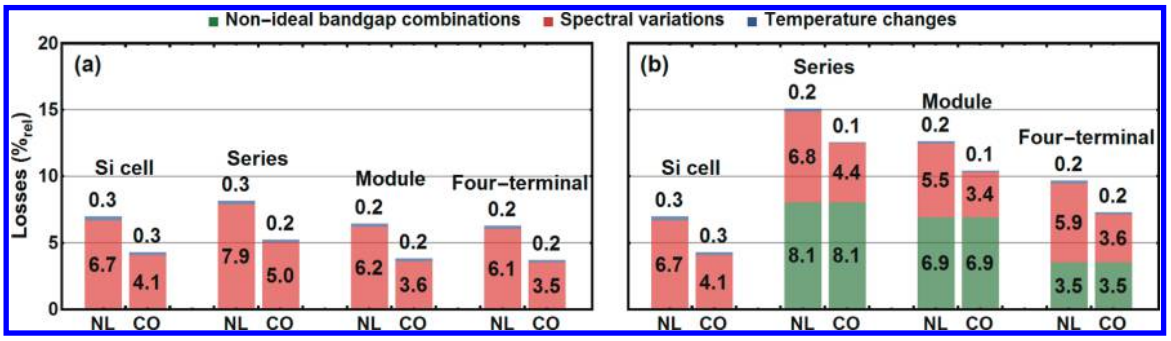

Figure 5. Effects of spectral variations, temperature changes, and the use of a nonideal perovskite band gap on the maximum power conversion efficiencies of the three perovskite/Si TSCs and a Si single-junction cell in NL[44] and CO[45] obtained by detailed-balance calculations for (a) the ideal perovskite band gap for the respective tandem configuration and (b) a perovskite band gap of 1.55 eV.

DOI: 10.1021/acsenergylett.6b00405
ACS Energy Lett. 2016, 1, 863−868

Temperature-dependent limiting efficiency, detailed-balance calculations, average photon energy, annually averaged spectra, irradiation-dependent limiting efficiency, optically thin perovskite/Si series tandem, experimental section, fitting procedure for measured spectra, and validation of the fitting procedure (PDF)

AUTHOR INFORMATION

Corresponding Author

*E-mail: b.ehrler@amolf.nl. Group homepage: https://amolf.nl/research-groups/hybrid-solar-cells.

Notes

Views expressed in this viewpoint are those of the author and not necessarily the views of the ACS.
Views expressed in this viewpoint are those of the authors and not necessarily the views of the ACS.
The authors declare no competing financial interest.

ACKNOWLEDGMENTS

The authors thank Eric C. Johlin, Mark W. Knight, Sander Mann, and Wilfried G. J. H. M. van Sark for comments on the manuscript. Furthermore, we thank Wilfried G. J. H. M. van Sark and Atse Louwen from the Utrecht Photovoltaic Outdoor Test facility (UPOT) and the NREL Solar Radiation Research Laboratory for providing spectral irradiance, ambient temperature, and relative humidity data. This work is part of the research program of the Foundation for Fundamental Research on Matter (FOM), which is part of The Netherlands Organization for Scientific Research (NWO).

REFERENCES

(1) Kojima, A.; Teshima, K.; Shirai, Y.; Miyasaka, T. Organometal Halide Perovskites as Visible-Light Sensitizers for Photovoltaic Cells. *J. Am. Chem. Soc.* **2009**, *131*, 6050−6051.

(2) Polman, A.; Knight, M.; Garnett, E. C.; Ehrler, B.; Sinke, W. C. Photovoltaic Materials: Present Efficiencies and Future Challenges. *Science* **2016**, *352*, aad4424.

(3) Green, M. A.; Emery, K.; Hishikawa, Y.; Warta, W.; Dunlop, E. D. Solar cell efficiency tables (version 48). *Prog. Photovoltaics* **2016**, *24*, 905−913.

(4) Tiedje, T.; Yablonovitch, E.; Cody, G. D.; Brooks, B. G. Limiting Efficiency of Silicon Solar Cells. *IEEE Trans. Electron Devices* **1984**, *31*, 711−716.

(5) Johnston, M. B.; Herz, L. M. Hybrid Perovskites for Photovoltaics: Charge-Carrier Recombination, Diffusion, and Radiative Efficiencies. *Acc. Chem. Res.* **2016**, *49*, 146−154.

(6) De Wolf, S.; Holovsky, J.; Moon, S.-J; Löper, P.; Niesen, B.; Ledinsky, M.; Haug, F.-J.; Yum, J.-H.; Ballif, C. Organometallic Halide Perovskites: Sharp Optical Absorption Edge and Its Relation to Photovoltaic Performance. *J. Phys. Chem. Lett.* **2014**, *5*, 1035−1039.

(7) Noh, J. H.; Im, S. H.; Heo, J. H.; Mandal, T. N.; Seok, S. I. Chemical Management for Colorful, Efficient, and Stable Inorganic-Organic Hybrid Nanostructured Solar Cells. *Nano Lett.* **2013**, *13*, 1764−1769.

(8) Noel, N. K.; Stranks, S. D.; Abate, A.; Wehrenfennig, C.; Guarnera, S.; Haghighirad, A.-A.; Sadhanala, A.; Eperon, G. E.; Pathak, S. K.; Johnston, M. B.; et al. Lead-Free Organic-Inorganic Tin Halide Perovskites for Photovoltaic Applications. *Energy Environ. Sci.* **2014**, *7*, 3061−3068.

(9) Pazos-Outón, L. M.; Szumilo, M.; Lamboll, R.; Richter, J. M.; Crespo-Quesada, M.; Abdi-Jalebi, M.; Beeson, H. J.; Vrućinić, M.; Alsari, M.; Snaith, H. J.; et al. Photon Recycling in Lead Iodide Perovskite Solar Cells. *Science* **2016**, *351*, 1430−1433.

(10) Vos, A. D. Detailed Balance Limit of the Efficiency of Tandem Solar Cells. *J. Phys. D: Appl. Phys.* **1980**, *13*, 839−849.

(11) Marti, A.; Araujo, G. Limiting Efficiencies for Photovoltaic Energy Conversion in Multigap Systems. *Sol. Energy Mater. Sol. Cells* **1996**, *43*, 203−222.

(12) Brown, A. S.; Green, M. A. Detailed Balance Limit for the Series Constrained two Terminal Tandem Solar Cell. *Phys. E* **2002**, *14*, 96−100.

(13) Brown, A. S.; Green, M. A. Limiting Efficiency for Current-Constrained Two-Terminal Tandem Cell Stacks. *Prog. Photovoltaics* **2002**, *10*, 299−307.

(14) White, T. P.; Lal, N. N.; Catchpole, K. R. Tandem Solar Cells Based on High-Efficiency c-Si Bottom Cells: Top Cell Requirements for > 30% Efficiency. *IEEE J. Photovolt.* **2014**, *4*, 208−214.

(15) Almansouri, I.; Ho-Baillie, A.; Green, M. A. Ultimate Efficiency Limit of Single-Junction Perovskite and Dual-Junction Perovskite/Silicon Two-Terminal Devices. *Jpn. J. Appl. Phys.* **2015**, *54*, 08KD04.

(16) Strandberg, R. Detailed Balance Analysis of Area De-Coupled Double Tandem Photovoltaic Modules. *Appl. Phys. Lett.* **2015**, *106*, 033902.

(17) Mailoa, J. P.; Bailie, C. D.; Johlin, E. C.; Hoke, E. T.; Akey, A. J.; Nguyen, W. H.; McGehee, M. D.; Buonassisi, T. A 2-terminal perovskite/silicon multijunction solar cell enabled by a silicon tunnel junction. *Appl. Phys. Lett.* **2015**, *106*, 121105.

(18) Bailie, C. D.; Christoforo, M. G.; Mailoa, J. P.; Bowring, A. R.; Unger, E. L.; Nguyen, W. H.; Burschka, J.; Pellet, N.; Lee, J. Z.; Grätzel, M.; et al. Semi-Transparent Perovskite Solar Cells for Tandems with Silicon and CIGS. *Energy Environ. Sci.* **2015**, *8*, 956−963.

(19) Werner, J.; Weng, C.-H.; Walter, A.; Fesquet, L.; Seif, J. P.; De Wolf, S.; Niesen, B.; Ballif, C. Efficient Monolithic Perovskite/Silicon Tandem Solar Cell with Cell Area > 1 cm^2. *J. Phys. Chem. Lett.* **2016**, *7*, 161−166.

(20) Albrecht, S.; Saliba, M.; Correa Baena, J. P.; Lang, F.; Kegelmann, L.; Mews, M.; Steier, L.; Abate, A.; Rappich, J.; Korte, L.; et al. Monolithic Perovskite/Silicon-Heterojunction Tandem Solar Cells Processed at Low Temperature. *Energy Environ. Sci.* **2016**, *9*, 81−88.

(21) Albrecht, S.; Saliba, M.; Correa-Baena, J.-P.; Jäger, K.; Korte, L.; Hagfeldt, A.; Grätzel, M.; Rech, B. Towards optical optimization of planar monolithic perovskite/silicon-heterojunction tandem solar cells. *J. Opt.* **2016**, *18*, 064012.

(22) Löper, P.; Moon, S.-J.; Martin de Nicolas, S.; Niesen, B.; Ledinsky, M.; Nicolay, S.; Bailat, J.; Yum, J.-H.; De Wolf, S.; Ballif, C. Organic-Inorganic Halide Perovskite/Crystalline Silicon Four-Terminal Tandem Solar Cells. *Phys. Chem. Chem. Phys.* **2015**, *17*, 1619−1629.

(23) Lang, F.; Gluba, M. A.; Albrecht, S.; Rappich, J.; Korte, L.; Rech, B.; Nickel, N. H. Perovskite Solar Cells with Large-Area CVD-Graphene for Tandem Solar Cells. *J. Phys. Chem. Lett.* **2015**, *6*, 2745−2750.

(24) Duong, T.; Lal, N.; Grant, D.; Jacobs, D.; Zheng, P.; Rahman, S.; Shen, H.; Stocks, M.; Blakers, A.; Weber, K.; et al. Semitransparent Perovskite Solar Cell With Sputtered Front and Rear Electrodes for a Four-Terminal Tandem. *IEEE J. Photovoltaics* **2016**, *6*, 679−687.

(25) McMeekin, D. P.; Sadoughi, G.; Rehman, W.; Eperon, G. E.; Saliba, M.; Hörantner, M. T.; Haghighirad, A.; Sakai, N.; Korte, L.; Rech, B.; et al. A Mixed-Cation Lead Mixed-Halide Perovskite Absorber for Tandem Solar Cells. *Science* **2016**, *351*, 151−155.

(26) Werner, J.; Barraud, L.; Walter, A.; Bräuninger, M.; Sahli, F.; Sacchetto, D.; Tétreault, N.; Paviet-Salomon, B.; Moon, S.-J.; Allebé, C.; et al. Efficient Near-Infrared-Transparent Perovskite Solar Cells Enabling Direct Comparison of 4-Terminal and Monolithic Perovskite/Silicon Tandem Cells. *ACS Energy Lett.* **2016**, *1*, 474−480.

(27) Chen, B.; Bai, Y.; Yu, Z.; Li, T.; Zheng, X.; Dong, Q.; Shen, L.; Boccard, M.; Gruverman, A.; Holman, Z.; Huang, J. Efficient Semitransparent Perovskite Solar Cells for 23.0%-Efficiency Perovskite/Silicon Four-Terminal Tandem Cells. *Adv. Energy Mater.* **2016**, 1601128.

(28) Sheng, R.; Ho-Baillie, A. W. Y.; Huang, S.; Keevers, M.; Hao, X.; Jiang, L.; Cheng, Y.-B.; Green, M. A. Four-Terminal Tandem Solar

DOI: 10.1021/acsenergylett.6b00405
ACS Energy Lett. 2016, 1, 863−868

Cells Using $CH_3NH3PbBr_3$ by Spectrum Splitting. *J. Phys. Chem. Lett.* **2015**, *6*, 3931−3934.
(29) Uzu, H.; Ichikawa, M.; Hino, M.; Nakano, K.; Meguro, T.; Hernández, J. L.; Kim, H.-S.; Park, N.-G.; Yamamoto, K. High efficiency solar cells combining a perovskite and a silicon heterojunction solar cells via an optical splitting system. *Appl. Phys. Lett.* **2015**, *106*, 013506.
(30) Masuko, K.; Shigematsu, M.; Hashiguchi, T.; Fujishima, D.; Kai, M.; Yoshimura, N.; Yamaguchi, T.; Ichihashi, Y.; Mishima, T.; Matsubara, N.; et al. Achievement of More Than 25% Conversion Efficiency with Crystalline Silicon Heterojunction Solar Cell. *IEEE J. Photovoltaics* **2014**, *4*, 1433−1435.
(31) Liu, H.; Ren, Z.; Liu, Z.; Aberle, A. G.; Buonassisi, T.; Peters, I. M. The Realistic Energy Yield Potential of GaAs-on-Si Tandem Solar Cells: a Theoretical Case Study. *Opt. Express* **2015**, *23*, A382−A390.
(32) Pazos, L. M.; Lee, J. M.; Kirch, A.; Tabachnyk, M.; Friend, R. H.; Ehrler, B. A Silicon-Singlet Fission Parallel Tandem Solar Cell Exceeding 100% External Quantum Efficiency. *arXiv* **2015**, *1512*, 07466.
(33) Lentine, A. L.; Nielson, G. N.; Okandan, M.; Cruz-Campa, J.-L.; Tauke-Pedretti, A. Voltage Matching and Optimal Cell Composition for Microsystem-Enabled Photovoltaic Modules. *IEEE J. Photovolt.* **2014**, *4*, 1593−1601.
(34) Strandberg, R. Spectral and Temperature Sensitivity of Area De-Coupled Tandem Modules. *Proceedings of the Photovoltaic Specialist Conference (PVSC) IEEE 42nd*; New Orleans, LA, June 14−19 2015; pp 1−6.
(35) Krishnan, P.; Schüttauf, J. W. A.; van der Werf, C. H. M.; Houshyani Hassanzadeh, B.; van Sark, W.G.J.H.M.; Schropp, R. E. I. Response to simulated typical daily outdoor irradiation conditions of thin-film silicon-based triple-band-gap, triple-junction solar cells. *Sol. Energy Mater. Sol. Cells* **2009**, *93*, 691−697.
(36) Louwen, A.; de Waal, A. C.; Schopp, R. E. I.; Faaij, A. P. C.; van Sark, W. G. J. H. M. Comprehensive characterisation and analysis of PV module performance under real operating conditions. *Prog. Photovoltaics* **2016**, Submitted for publication.
(37) Shockley, W.; Queisser, H. J. Detailed Balance Limit of Efficiency of p-n Junction Solar Cells. *J. Appl. Phys.* **1961**, *32*, 510−519.
(38) Kottek, M.; Grieser, J.; Beck, C.; Rudolf, B.; Rubel, F. World Map of the Köppen-Geiger Climate Classification Updated. *Meterol. Z.* **2006**, *15*, 259−263.
(39) Betts, T. R.; Jardine, C. N.; Gottschalg, R.; Infield, D. G.; Lane, K. Impact of Spectral Effects on the Electrical Parameters of Multijunction Amorphous Silicon Cells. *Proceedings of the 3rd World Conference on Photovoltaic Energy Conversion*; Osaka, Japan, 2003; pp 1756−1759 Vol.2.
(40) Minemoto, T.; Nakada, Y.; Takahashi, H.; Takakura, H. Uniqueness Verification of Solar Spectrum Index of Average Photon Energy for Evaluating Outdoor Performance of Photovoltaic Modules. *Sol. Energy* **2009**, *83*, 1294−1299.
(41) Liu, H.; Aberle, A. G.; Buonassisi, T.; Peters, I. M. On the methodology of energy yield assessment for one-Sun tandem solar cells. *Sol. Energy* **2016**, *135*, 598−604.
(42) Louwen, A.; de Waal, A. C.; van Sark, W.G.J.H.M. Evaluation of different indicators for representing solar spectra. *Proceedings of the Proc. 43rd IEEE PV specialist conference*; Portland, OR, June 5−10 2016, in press.
(43) Kasten, F.; Young, A. T. Revised Optical Air Mass Tables and Approximation Formula. *Appl. Opt.* **1989**, *28*, 4735−4738.
(44) van Sark, W. G. J. H. M.; Louwen, A.; de Waal, A. C.; Schropp, R. E. I. UPOT: the Utrecht Photovoltaic Outdoor Test facility. *Proceedings of the 27th European Photovoltaic Solar Energy Conference*; Frankfurt, DE, September 24−28 2012; pp 3247−3249.
(45) Andreas, A.; Stoffel, T. *NREL Solar Radiation Research Laboratory (SRRL): Baseline Measurement System (BMS); Golden, Colorado (Data)*; NREL Report No. DA-5500-56488; NREL: Golden, CO, 1981.
(46) Nann, S.; Riordan, C. Solar Spectral Irradiance under Clear and Cloudy Skies: Measurements and a Semiempirical Model. *J. Appl. Meteorol* **1991**, *30*, 447−462.
(47) Bohren, C. F. *Atmospheric Optics, The Optics Encyclopedia*; Wiley-VCH, 2007.
(48) Hulburt, E. O. Explanation of the Brightness and Color of the Sky, Particularly the Twilight. *J. Opt. Soc. Am.* **1953**, *43*, 113−118.
(49) Dave, J. V.; Sekera, Z. Effect of Ozone on the Total Sky and Global Radiation Received on a Horizontal Surface. *J. Meteorol.* **1959**, *16*, 211−212.

DOI: 10.1021/acsenergylett.6b00405
ACS Energy Lett. 2016, 1, 863−868